A numerical simulation of avascular tumour growth

Tan Liang Soon*   Ang Keng Cheng*

(Received 27 October 2004, revised 11 August 2005)

Abstract

We develop and calibrate a mathematical model for avascular tumour growth. The model is formulated as a set of partial differential equations describing the spatio-temporal changes in cell concentrations based on reaction-diffusion dynamics and the law of mass conservation. Unlike existing models, the current model takes into account the dependence of the cell proliferation rate on the growth inhibiting factors secreted by necrotic cells; furthermore, the model incorporates an element of random variation to the mitotic rate and nutrient supply. The model is solved using standard finite difference techniques. Results obtained from the simulation compare well with published experimental data. The biological and clinical implications of these results are also discussed.

---

*National Institute of Education, Nanyang Technological University, 1 Nanyang Walk, Singapore 637616. mailto:shan@ri.sch.edu.sg

Contents

1   Introduction

The development of a primary solid tumour begins with a single normal cell becoming transformed as a result of mutations in certain key genes. This transformed cell differs from a normal one in its escape from the body's homeostatic mechanisms, leading to inappropriate proliferation and a tendency to override apoptosis or cell death. An individual tumour cell has the potential, over successive divisions, to develop into a cluster of tumour cells. Further growth and proliferation leads to the development of an avascular tumour consisting of approximately 10^6 cells which feed on oxygen and other nutrients present in the local environment.

After the early stages of growth, the avascular spheroids consist structurally of an inner zone of necrotic cells (dead due to lack of nutrients) and an outer zone of living cells. This outer zone is further divided into a layer largely composed of quiescent cells and a layer largely composed of proliferating cells; although dead cells are also found adjacent to both quiescent and proliferating cells (Sutherland [8]).

In recent years several mathematical models, using different approaches, have been developed to describe the features of avascular tumour growth. Following experimental observations that the transitions between layers of tumour cells are more likely to be gradual than sharp (Hystad & Rofstad [6]), some of these models used a continuum, macroscopic framework in one space dimension (Ward & King [9, 10]). Sherratt & Chaplain [7] examined the implications of incorporating random cell movement into the continuum of live tumour cells on avascular tumour growth. More recently, Ang & Tan [1] proposed and developed a mathematical model based on the modelling framework presented in Sherratt & Chaplain for the study of avascular tumour growth with random variation. This model succeeds in giving a more realistic mathematical description of avascular tumour growth; however, the arbitrary choice for the mitotic rate parameter provides little quantitative understanding of the dynamics of cell growth.

In order to understand the underlying dynamics of cell growth within a spheroid, Nirmala et al. [3] studied the spatio-temporal distribution of the cells in spheroids cultured from SNB19, a high grade glioblastoma cell line. To determine the size of the spheroids and its growth rate, they are stained with trypan blue. A hemacytometer was used under a light microscope to count the number of live (trypan blue excluding) and dead cells. A set of experiments was designed to investigate the change of the cell count and volume with respect to time. They found that the size of the spheroids and their growth rates were dependent on the cell number, the proliferation was mostly limited to the outermost region as the spheroids grew in size, and the number of dead cells increased with age and size as well.

Mechanical effects from the surrounding environment as well as that generated internally by cellular growth play an important role in regulating tumour growth. Evidence that cell stress affects proliferation is provided by Helmlinger et al. [5]. By culturing spheroids in gels of different stiffness, it was demonstrated that the stress exerted on tumour cells by their surroundings affects its equilibrium size. High stress is observed to down-regulate

cell proliferation and promote cell death. A common feature of mathematical models on tumour growth is that they have assumed that the tumour cells are of the same type for the simplicity of closing the system of mass balance equations. This approach does not permit the investigation of the chematic effects that different clones of cells (for example, cells with different expression of the tumour suppressor gene p53) have on the morphology of the vascular environment, and hence, the nutrient supply. An element of random variation to the mitotic rate and nutrient supply have been incorporated into the model proposed here and are discussed in Ang & Tan [1].

We attempt to assess the quantitative accuracy of the model in Ang & Tan [1] by comparing numerical results for varying values of the mitotic rate parameter with independent experimental data on the dynamics of cell growth from Nirmala et al. [3] Unlike the model in Ang & Tan, the model analysed here devises a method to provide a reasonably realistic parameter value for the mitotic rate. The response of the calibrated model to varying levels of the nutrient supply is examined for its biological and clinical implications. We observe that the predicted tumour cell distribution in the current model is not smooth and no tumour regression is demonstrated.

2   Model formulation

See in the schematic diagram presented in Figure 1 that we treat the *in vivo* tumour as a continuum of proliferating, quiescent and necrotic cells, whose densities are denoted by $p(x,t)$, $q(x,t)$ and $n(x,t)$ respectively, where t and x are the time and the one dimensional spatial coordinate respectively.

Assume the nutrients pass through the surface of the tumour and diffuse into the interior through the intracellular space sufficiently fast enough that the local nutrient concentration $c(x,t)$ is quasi steady. Since the Gompertz growth rate was reported in many experimental studies, we postulate that the mitosis rate $g(c)$ of the proliferating cells depends on $c(x,t)$ of nutrients with
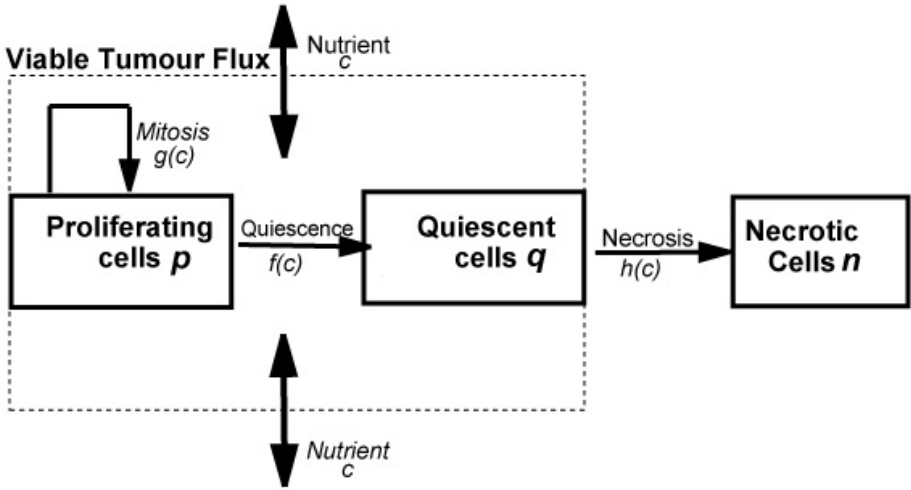
FIGURE 1: A schematic diagram of the interaction between the proliferating, quiescent and necrotic cell densities.

a Gompertzian representation. In addition to the crowding effects of the total cell population, the model includes the effects of mitotic inhibitors secreted from the necrotic site (as described by Freyer [4]) in a growth retardation term of $I(n)$, assumed to be proportional to the necrotic cells density. In the direction of the core of the tumour, some proliferating cells with limited access to the intracellular nutrients become quiescent at rate $f(c)$ and some quiescent cells which are totally deprived of nutrients undergo necrosis at rate $h(c)$.

The suggested model in Sherratt & Chaplain [7] for the interaction between the proliferating and quiescent cells, namely

$$\frac{\partial}{\partial x}\left[\frac{p}{p+q}\frac{\partial(p+q)}{\partial x}\right] \quad \text{and} \quad \frac{\partial}{\partial x}\left[\frac{q}{p+q}\frac{\partial(p+q)}{\partial x}\right],$$

respectively, is used in the current model. The overall viable cell flux $\frac{\partial}{\partial x}(p+q)$ as illustrated in Figure 1 is fractionated evenly between the proliferating and

quiescent cells densities. This captures the phenomenological effect of contact inhibition in the random motility of tumour cells where the two cell populations presumably have equal motility. Mass conservation is also applied to the cells.

With mass conservation applied to the cells, the set of Sherratt & Chaplain's [7] equations governing the evolution of $p(x,t)$, $q(x,t)$, $n(x,t)$ and $c(x,t)$ are:

$$\frac{\partial p}{\partial t} = \frac{\partial}{\partial x}\left[\frac{p}{p+q}\frac{\partial\left(p+q\right)}{\partial x}\right] + g(c)p(1-p-q-n) - \left(f(c)+I(n)\right)p\,; \quad (1)$$

$$\frac{\partial q}{\partial t} = \frac{\partial}{\partial x}\left[\frac{q}{p+q}\frac{\partial\left(p+q\right)}{\partial x}\right] + f(c)p - h(c)q\,; \quad (2)$$

$$\frac{\partial n}{\partial t} = h(c)q\,; \quad (3)$$

$$c = \frac{c_0\gamma}{\gamma+p}\left[1-\alpha\left(p+q+n\right)\right]\,. \quad (4)$$

Equation (4) represents the access of nutrient from underlying tissue. By assuming that the effectiveness of this source term decreases with overall cell density, the parameter $\alpha \in (0,1]$ represents a constant of proportionality and c_0 is the nutrient concentration in the absence of a tumour cell population. We assume that the cells are completely close-packed at the maximum non-dimensionalised cell density of 1. Moreover, assume the functions $f(c)$ and $h(c)$ decrease with $f\left(+\infty\right) = h\left(+\infty\right) = 0$.

The system of equations (1–4) is first discretised using forward differencing for time and central differencing for space:

$$p_i^{j+1} = \Delta t\left[u_i^j + g(c_i^j)p_i^j\left(1-p_i^j-q_i^j-n_i^j\right) - \left(f(c_i^j)+I(n_i^j)\right)p_i^j\right] + p_i^j\,, \quad (5)$$

$$q_i^{j+1} = \Delta t\left[v_i^j + f(c_i^j)p_i^j - h(c_i^j)q_i^j\right] + q_i^j\,, \quad (6)$$

$$n_i^{j+1} = n_i^j + \Delta t\left(h(c_i^j)q_i^j\right)\,, \quad (7)$$

$$c_i^j = \frac{\gamma}{\gamma+p_i^j}\left[1-\alpha\left(p_i^j+q_i^j+n_i^j\right)\right]\,, \quad (8)$$

where

$$u_i^j = \frac{(p_{i+1}^j - p_{i-1}^j)r_i^j(r_{i+1}^j - r_{i-1}^j) + 4p_i^j r_i^j(r_{i+1}^j - 2r_i^j + r_{i-1}^j) - p_i^j(r_{i+1}^j - r_{i-1}^j)^2}{4(\Delta x)^2 (r_i^j)^2}$$

$$v_i^j = \frac{(q_{i+1}^j - q_{i-1}^j)r_i^j(r_{i+1}^j - r_{i-1}^j) + 4q_i^j r_i^j(r_{i+1}^j - 2r_i^j + r_{i-1}^j) - q_i^j(r_{i+1}^j - r_{i-1}^j)^2}{4(\Delta x)^2 (r_i^j)^2}$$

and $r_i^j = p_i^j + q_i^j$. The increments Δt and Δx refer to the time intervals and space steps respectively in the finite difference scheme. In the above set of finite difference equations, the superscript represents the time level and the subscript represents the space position.

Since cell stress affects proliferation, assume that moderate stress promote cell division whereas low and high stress down-regulate cell proliferation and promote cell death. Furthermore, assume that cell velocity correlate with the tumour expansive forces, which then contributes to the cellular stress. The experimental fit for the average cell velocity in the form of the Gamma distribution (Balazs et al. [2]) leads us to use a rescaled Gamma distribution term v_p, to model the random dependence of the cell proliferation rate on the cellular stress. Hence equation (5) becomes

$$\begin{aligned}
p_i^{j+1} &= \Delta t \left[u_i^j + \left(g(c_i^j) + v_p \right) p_i^j \left(1 - p_i^j - q_i^j - n_i^j \right) - \left(f(c_i^j) + I(n_i^j) \right) p_i^j \right] \\
&\quad + p_i^j \, .
\end{aligned} \tag{9}$$

The tumour is also assumed to contain several functionally-disparate clones of tumour cells, so that there exists the random collapse and regrowth of blood vessels in the tumour. In order to simulate the alternating levels of nutrients in parallel with this random variation in the tumour vascular environment, we incorporate a rescaled Normally distributed random term v_c to the quasi steady nutrient term. We obtain these random numbers from a Normal distribution rather than a uniform distribution as it is more likely that this variation will not remain uniform throughout time. Hence equa-

tion (8) becomes

$$c_i^j = v_c + \frac{\gamma}{\gamma + p_i^j}\left[1 - \alpha\left(p_i^j + q_i^j + n_i^j\right)\right].$$

(10)

The initial and boundary conditions are:

- Boundary conditions at $x = 0$ and $x = 210$ are

$$\frac{\partial p}{\partial x} = 0,$$

(11)

$$\frac{\partial q}{\partial x} = 0;$$

(12)

- Initial conditions for $x \in [0, 210]$ are

$$q(x, 0) = n(x, 0) = 0,$$

(13)

$$p(x, 0) = e^{-0.1x}.$$

(14)

p and q are defined so that $p + q$ is non-zero everywhere initially. This then provides the initial conditions for a properly defined model. The small initial proliferating cell density (0.01) at the centre of the tumour corresponds to the early stages of tumour growth. The condition at the artificial boundary of $x = 210$ is necessary to provide a finite domain for numerical computations. It is required because we cannot solve numerically on a semi-infinite domain.

In the numerical solution of the discrete finite difference equations (6), (7), (9) and (10), the parameter values as given in the model developed by Sherratt & Chaplain [7] are $\gamma = 10$, $c_0 = 1$ and $\alpha = 0.05$, with $f(c) = \frac{1}{2}(1 - \tanh(4c - 2))$, $g(c) = \beta e^{\beta c}$, $h(c) = \frac{1}{2}f(c)$ and $I(n) = \frac{1}{2}n$. Here, β in the function $g(c)$ serves as a parameter for calibration of the model.

In solving the finite difference equations, Δt and Δx are set at 0.1 and 1 respectively. The first part involves the use of Microsoft EXCEL 2000 to

generate a set of random numbers for v_p from a Gamma distribution $\chi \sim \Gamma(0.5, 1)$. A pseudo random number generator is also used to generate the set of random numbers for v_c from a Normal distribution with mean 0 and variance 0.04. Computation was stable for the chosen set of of parameters and convergence was rapid.

3 Model calibration

Nirmala et al. [3] recorded the diameter measurement and cell counts individually for six spheroids every week for a period of four weeks. The results, presented in Figure 2, show an exponential growth pattern of the average volume and total cell count with respect to time.

Figure 2 compares the predictions of the models with the measured cell count of the live, dead and total cell population. In these calibration experiments, the cell density data from the model are fitted by choosing an appropriate scaling factor to transform the model's cell density to cell count. The mean absolute relative error (between the model and experimental data) against varying β values from 0.1 to 1.0 are then computed. The results presented in Figure 3 show that the model having a β value of 0.3 and a corresponding minimum mean absolute relative error of 0.184725 gives an optimal estimate to the experimental cell count data.

Figure 4 depicts the comparison of the live, dead and total cell count between the calibrated model and the experimental data. In general, the results show the model performs well when compared to the experimental results for $t = 1$ to $t = 3$. The model did not give a satisfactory prediction to the higher experimental cell count at $t = 4$. We attribute this to the fact that both model and experiment have errors. The nutrient feed in the experimental laboratory setting is also different from that of the model and it is possible that the experimental tumour cultured under such conditions will outgrow in week 4.
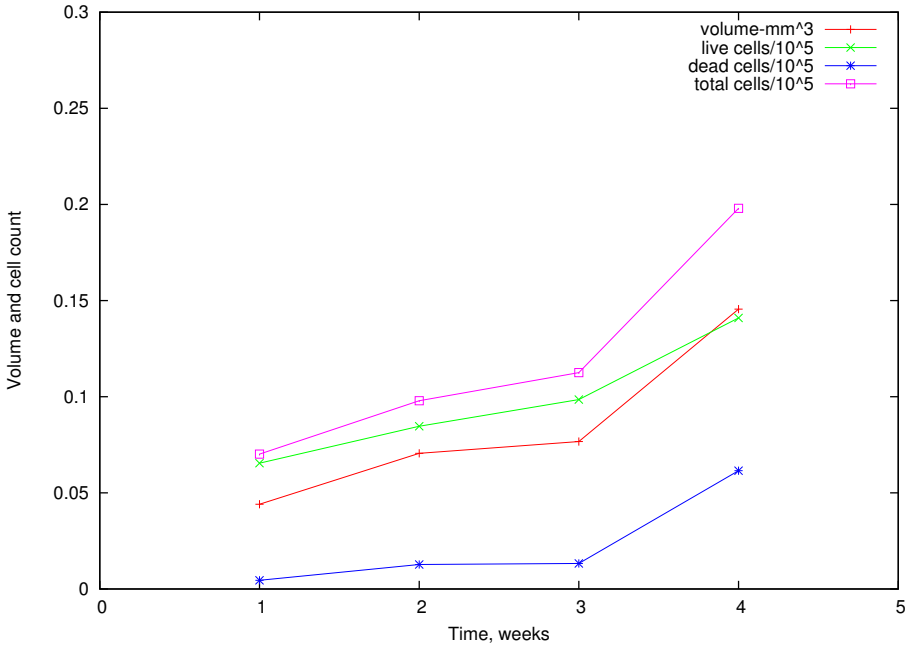
FIGURE 2: The average cell counts (live, dead and total) and volume of five spheroids at each week. Data reproduced from Nirmala et al. [3], with permission.

4 Results and discussion

The calibrated model is solved for the set of parameters, functions, boundary and initial values mentioned above. Red blood cell distribution flows inhomogeneously through the normal vasculature in the body tissue. Hence, values of α ranging from 0.4 to 0.8 were used in the simulation runs to investigate how the variability in the nutrient supply affects its growth dynamics. A range of linear, quadratic and exponential functional forms for $I(n)$ were also tested. From the computational experiments, it appears that the most reasonable set of results was obtained when $I(n)$ was chosen to be a linear
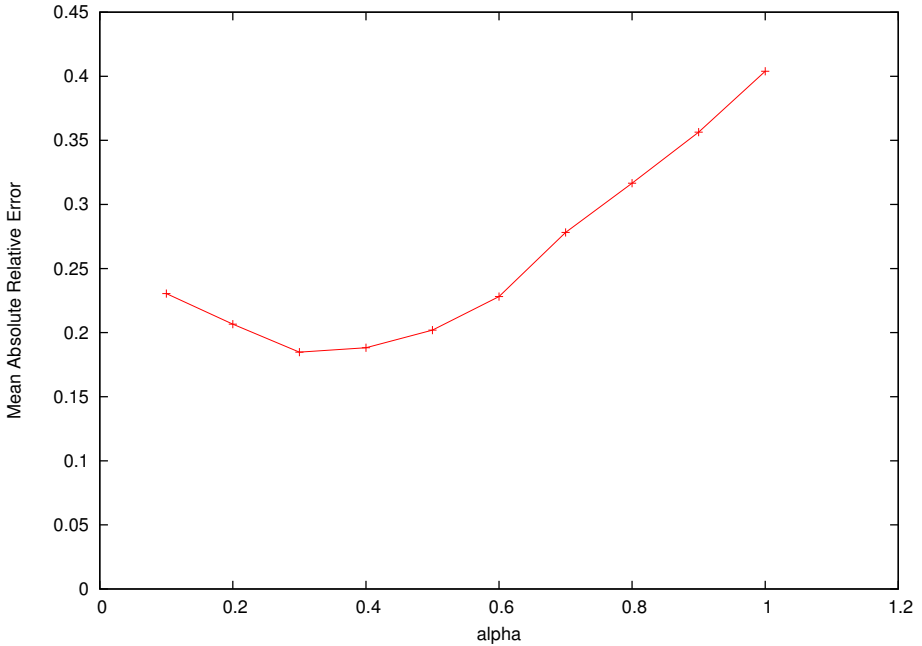
FIGURE 3: A distribution of the mean absolute relative error for β values from 0.1 to 1.0 .

function, such as $I(n) = \frac{1}{2}n$. Due to space constraints, only results of the simulations for cases when $\alpha = 0.4$ and $\alpha = 0.8$ are presented and discussed here.

The tumour in Ang & Tan [1] model is treated on a macroscopic perspective, in which the spatio-temporal dynamics of cell concentrations are modelled based on reaction-diffusion dynamics and mass conservation law. It included the dependence of the cell proliferation rate on the growth inhibiting factors secreted by necrotic cells and the incorporation of random variation to the mitotic rate and nutrient supply. The model in Ang & Tan predicted a smooth and asymmetric spatial tumour cell distribution. Just as in the Ang & Tan model, the results presented in Figure 5(a)–7(a) show
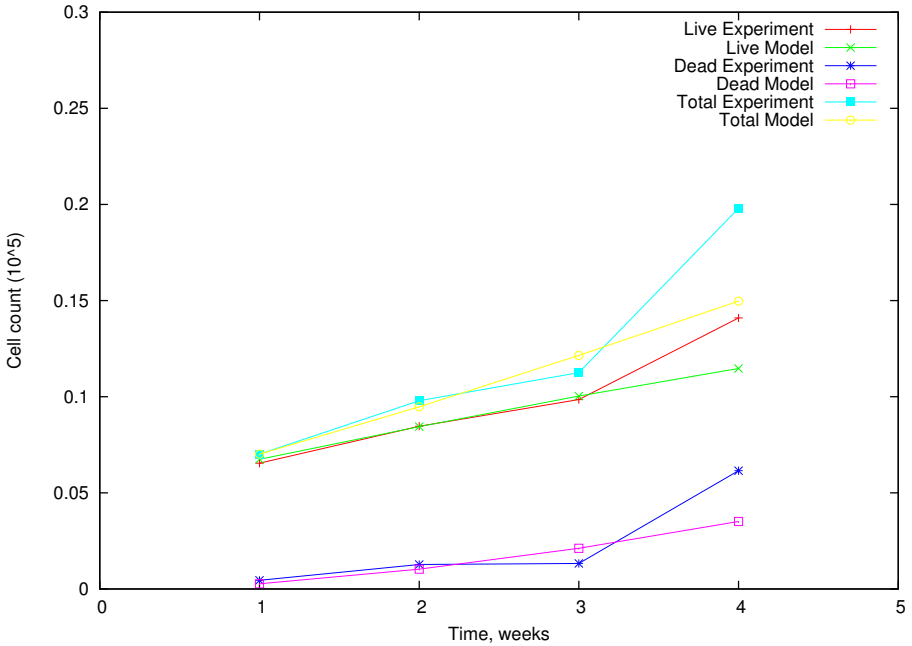
FIGURE 4: Comparison of the live, dead and total cell count between the calibrated model and the experimental data.

that the symmetry of the tumour cell distribution as observed in the model developed by Sherratt & Chaplain [7] is broken and there is now an asymmetric spatial distribution of an advancing pulse of proliferating cells (p), with a band of quiescent cells (q) and a necrotic core (n) behind this in a radial direction at time steps $t = 0, 2, 4, \ldots, 14$.

Unlike the model in Ang & Tan [1], observe in Figure 5–7 that the predicted tumour cell distribution in the current model is not smooth. This indicates that the cell density is not a constant with respect to time or position. These results suggest that the tumour cells may be constantly reorganising themselves within the tumour.

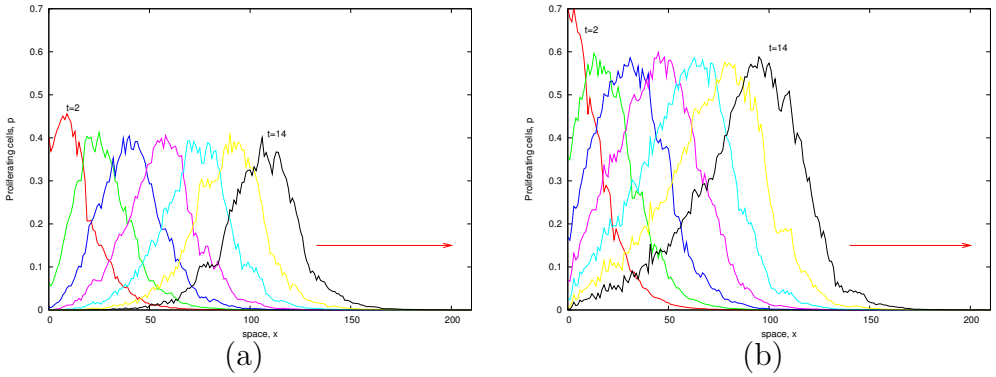The observed growth differences between the tumour subpopulations of

FIGURE 5: A numerical solution with (a) $\alpha = 0.8$ and (b) $\alpha = 0.4$, plotted as a function of space at times $t = 0, 2, 4, \ldots, 14$ for Proliferating cells.

proliferating, quiescent and necrotic cells could be attributed to the heterogeneity in each of their own growth dynamics. Note that no tumour regression is demonstrated, in that as time evolves, despite the necrotic cells density building up, the proliferating and quiescent cells are still propagating with no observed decrease in densities. These results are in good agreement with the analysis performed on the experimental data. Nirmala et al. [3] reported that they did not observe a limiting spheroid volume. Instead, they observed growth of the total volume of the spheroid over time. Hence, other than the diffusion limited nutrient supply and the production of mitotic inhibitors as assumed in the model, other factors such as cell stress and the variation in the tumour vascular environment may regulate its growth characteristics.

Figures 5(b)–7(b) show that as α is decreased, and hence driven forward by the increased access of nutrient from the surrounding tissues of another body site, a larger proportion of the tumour cells proliferate, so that the layer of live tumour cells thickens and the necrotic core diminishes in size. In addition, as time evolves, Figure 5(b) shows a small buildup of proliferating cells in the necrotic core, indicating an active proliferative state of the tumour. Differences in the tumour growth dynamics at different body sites suggests
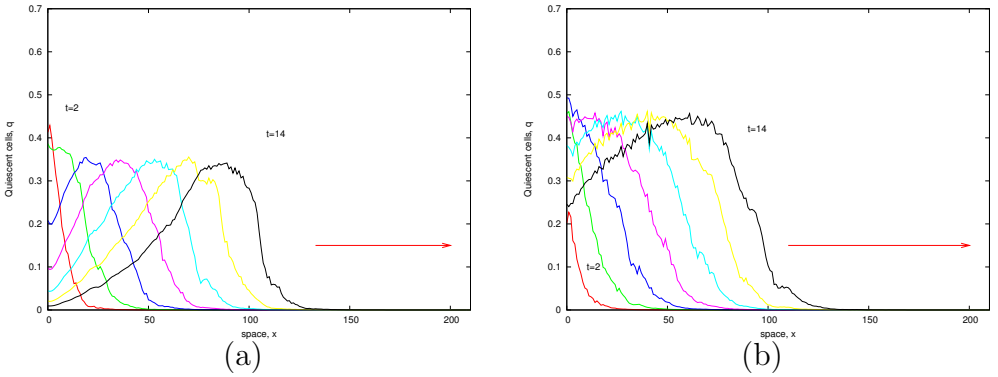
FIGURE 6: A numerical solution with (a) $\alpha = 0.8$ and (b) $\alpha = 0.4$, plotted as a function of space at times $t = 0, 2, 4, \ldots, 14$ for Quiescent cells.

that it may be improper to interpret results obtained with therapeutic agents restricted only to tumour growth at a particular body site.

Despite becoming more proliferative in the presence of a simulated rich supply of nutrient, the tumour expansion rate is observed to be unaffected in Figure 5–7. Results from the present model indicate that tumour growth is influenced not only by the availability of nutrients, but also by the random intracellular stress effects on cell proliferation rate, v_p, as well as random variation in the nutrient level, v_c.

5   Conclusion

The model presented in this paper focuses on the quantitative description of the dynamics of avascular tumor growth. The model provides a strategy to incorporate a realistic model and allows it to be fitted against experimental data. However, this model may be generalised to allow for stochastic effects on the mitotic rate and nutrient level. The use of stochastic par-
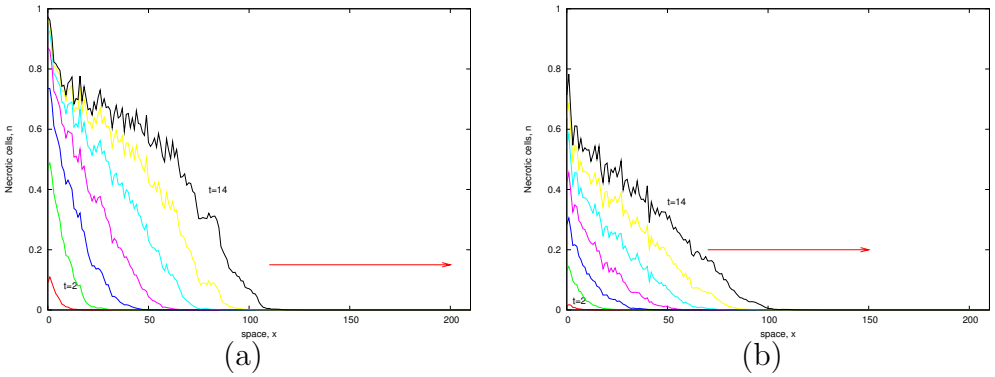
FIGURE 7: A numerical solution with (a) $\alpha = 0.8$ and (b) $\alpha = 0.4$, plotted as a function of space at times $t = 0, 2, 4, \ldots, 14$ for Necrotic cells.

tial differential equations in such models is currently being considered by the authors. We hope that the quantitative results from the present model will provide clinical practitioners with valuable information on the potential effects of novel therapies and their exact schedules. These could represent future therapeutic targets to be manipulated in managing the disease.

References

[1] Ang, K. C. and Tan, L. S.: An avascular tumour model with random variation, *8th ATCM conference proceedings*, **1**, 153–161 (2003). http://epatcm.any2any.net/EP/2003/2003C173/abstract.html C904, C905, C912, C913

[2] Balazs, H., Andraz, C., Ilona, F., Tamas, M., Emilia, M. and Tamas, V.: Locomotion and proliferation of glioblastoma cells *in vitro*: statistical evaluation of videomicroscopic observations. *J. Neurosurg.*, 92, 428–434 (2000). http://angel.elte.hu/pdf/glioma.pdf C908

[3] Chandrasekar, N., Jasti S. R., Arnout C. R., Lauren A. L.and Mandri, O.: Growth characteristics of glioblastoma spheroids, *Int. J. Oncology*, **19**, 1109–1115 (2001). C904, C905, C910, C911, C914

[4] Freyer, J. P.: Role of necrosis in regulating the growth saturation of multicellular spheroids, *Cancer Res.*, **48**, 2432–2439 (1988). http://cancerres.aacrjournals.org/cgi/content/abstract/48/9/2432 C906

[5] Helmlinger, G., Netti, P. A., Lichtenbeld, H. C., Melder, R. J. and Jain R. K.: Solid stress inhibits the growth of multicellular tumor spheroids, *Nature Biotech*, **15**, 778–783 (1997). http://dx.doi.org/10.1038/nbt0897-778 C904

[6] Hystad, M. E., Rofstad, E. K.: Oxygen consumption rate and mitochondrial density in human melanoma monolayer cultures and multicellular spheroids, *Int. J. Cancer*, **57**, 532–537 (1994). C904

[7] Sherratt, J. A., Chaplain, M. A. J.: A new mathematical model for avascular tumour growth, *J. Math. Biol.*, **43**, 291–312 (2001). http://dx.doi.org/10.1007/s002850100088 C904, C906, C907, C909, C913

[8] Sutherland, R. M.: Cell and environment interaction in tumour microregions: The multicell spheroid model, *Science*, **240**, 177–184 (1988). C903

[9] Ward, J. P., King, J. R.: Mathematical modelling of avascular tumour growth, *IMA J. Math. Appl. Med. Biol.*, **14**, 39–70 (1997). http://dx.doi.org/10.1093/imammb/14.1.39 C904

[10] Ward, J. P., King, J. R.: Mathematical modelling of avascular-tumour growth II: modelling growth saturation, *IMA J. Math. Appl. Med. Biol.*, **16**, 171–211 (1999). http://dx.doi.org/10.1093/imammb/16.2.171 C904